Applied Energy 377 (2025) 124621

Contents lists available at ScienceDirect

Applied Energy

journal homepage: www.elsevier.com/locate/apenergy

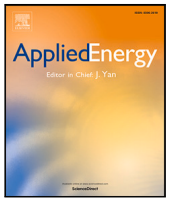

Novel abstractions and experimental validation for digital twin microgrid design: Lab scale studies and large scale proposals

Md. Mhamud Hussen Sifat [a,*], Safwat Mukarrama Choudhury [a], Sajal K. Das [a], Hemanshu Pota [b], Fuwen Yang [c]

[a] Rajshahi University of Engineering & Technology, Kajla, Rajshahi, 6204, Bangladesh
[b] University of New South Wales, Canberra, Australia
[c] Griffith University, Gold Coast, Queensland, Australia

ARTICLE INFO

Keywords:
Digital twin microgrid control
Energy management
Self-healing
Microgrid optimization

ABSTRACT

Managing the current high penetration of renewable energy sources globally poses a significant challenge due to the distributed and diverse nature of generation components. To maximize real-time power generation, these resources need to perform optimally. Digital twin technology offers a comprehensive framework for managerial support by replicating grid features in a digital environment. This research creates a digital twin of the microgrid to optimize power generation, focusing on computational efficiency and self-healing control. The framework is tested in a laboratory microgrid, with modeling performed using a polynomial regression algorithm. Optimization is achieved through a gradient descent algorithm, and the self-healing model is implemented using a logistic regression algorithm. Real-time data extracted from the microgrid drives this process. The results can be utilized for predictive analysis before deploying a microgrid or to optimize generation in existing systems using the digital twin model. Even though the research focuses on a single microgrid unit, it introduces a framework proposal for extensively distributed microgrids integrating multiple renewable energy sources.

1. Introduction

The utilization of microgrids has witnessed a significant surge in recent times, primarily due to the global fuel crisis and the pressing issue of global warming [1,2]. The primary drivers for the widespread adoption of microgrids include the cost-effective generation of energy, the operational flexibility in both grid-connected and islanded modes and the ability to have distributed control [3]. The microgrid concept has evolved significantly in the present era, demonstrating enhanced development and organization [4]. Moreover, there is a growing trend toward the adoption of advanced power systems such as virtual power plants (VPPs) and smart grids (SGs) [5,6]. The VPPs and SGs incorporate an increasing number of devices, thereby making it essential to have larger area control, sensor network management, and ensure sustainability. The intelligent use of these technologies will be vital for the overall system management and control of energy in the future [7].

The increasing number of grid components inside MGs has increased the number of parameters, which can have a substantial impact on the control and administration of the huge volumes of data created by these systems [8,9]. The challenges that this fast-developing energy solution is now confronting include sustainable management, optimum control, failure prediction, renewables integration, and coping with uncertainty [10]. These issues must be solved to enable future MG management with a greater number of distributed energy resources (DERs). Sustainable MG management is critical for lowering the carbon footprint and environmental effects of MGs [11]. Optimal control of MGs is required to achieve optimal resource usage and energy management. Failure prediction is crucial for avoiding system downtime while considering renewables integration is critical for improving the sustainability of MGs [12].

The rise of digital twin technology is a game changer in this area since the challenges are enormous when compared to previous distributed control systems [13]. A digital twin digitally replicates a system, and the replica may now be utilized to examine system capabilities and input–output characteristics [14]. The system efficiently performs large-scale system control and data management throughout a device's lifespan. The technology's characteristics provide sustainability in terms of control, resource usage, and uncertainty handling since it continually monitors system behavior [15,16]. This system stores data on the cloud for real-time monitoring and historical data analysis. The

* Corresponding author.
E-mail address: asifat331@gmail.com (M.M.H. Sifat).

https://doi.org/10.1016/j.apenergy.2024.124621
Received 7 June 2024; Received in revised form 9 September 2024; Accepted 30 September 2024
Available online 8 October 2024

Nomenclature

$(V, I)_{Ld}$	Load voltage and current.
γ^i_{dr}	Unoptimized outputs.
Γ^i_{out}	Optimized outputs.
λ^i_{dr}	Unoptimized MG input parameters $\lambda_0, \lambda_1, \lambda_3,$ ..., λ_n for distributed energy resource.
Λ^i_{in}	Optimized MG inputs.
Y^i_{sts}	Actuation outputs for health states ζ^i_{dr}.
ζ^i_{dr}	System supporting health states.
ζ^i_{act}	Physical grid states notation.
ζ^i_{dt}	DT grid acquired states: updated in real-time via grid sensors network.
C_c	Net computation cost.
e_t	Real-time model error.
M_c	Model constraints.
M_{lf}	Model life-cycle constraint.
M_{lt}	Model linearity constraint.
$P^{pv/wt}_{act}$	Generated power of the renewables.
$P^{pv/wt}_{pre}$	Model predicted power.
$P^{pv/wt}_{t++}$	Power at $t+1$ which is updated in real-time as $P^{pv/wt}_{t++} \leftarrow P^{pv/wt}_{t}$.
P_{MG}	Integrated digital model of an MG including P^{PV} and P^{WT}.
P_{PV}	Digital model of a PV module.
P_{WT}	Digital model of a Wind turbine.
BESS	Battery energy storage system.
CSTM	Component-specific twin model.
DERs	Distributed energy resources.
DM	Digital model.
DS	Digital Shadow.
DT	Digital twin.
DTEG	Digital twin electric grid.
DTMG	Digital twin microgrid (MG).
DTMG	Digital twin microgrid.
ESS	Energy storage system.
MG	Microgrid.
RESs	Renewable energy sources.
SG	Smart grid.

predictive maintenance function assists in selecting appropriate output profiles to ensure sustainability [17,18].

This study systematically creates a digital twin of an MG, from component-level modeling to final framework testing. The design adheres to the operational and control procedures of an operational DT, considering both the digital twin concept and MG characteristics. DER modeling is employed initially, utilizing a polynomial regression algorithm on the MG unit datasets. Logistic regression is used for fault case classification and triggering output. In terms of operation and control, both the physical grid and the twin grid are integrated for the performance test. Despite the variety of algorithms available for modeling an MG component's inputs and outputs, the optimization problem generally favors computationally efficient methods. With these algorithms, the model's performance remains satisfactory.

Digital twin technology aids in resolving centralized and decentralized management challenges in complex infrastructures. While traditional grid component hierarchies remain, the DT layer is added as an advanced control layer retrofit. Standardization involves systematic development with both system-level and component-level abstractions. The lower-level hierarchy prioritizes initial digital model development, representing grid variables in a stationary state mapping. The model's features align with its intended functionality as shown in Table 1. This paper utilizes ML-based models for power forecasting, control systems, and framework optimization. Integration of models enables multiple grid components to operate in parallel with real-time bidirectional communication features.

The Contributions of this work are as follows:

- Introduces a data-driven modeling approach to establish a digital twin for a microgrid.
- Demonstrates generation optimization and self-healing using the developed digital twin microgrid.
- Lays the foundation for large-scale microgrid system applications.

The rest of the paper progresses from modeling to demonstrations of a functional DT microgrid. Section 2 provides the background of this work, discussing the current state of research and related studies on digital twin microgrids. The DT modeling for the specific devices utilized in the current lifespan is described in Section 3. Theoretical aspects of framework model-associated methodologies are provided here. The implementation procedure of the theoretical framework is presented in Section 4. Section 5 presents operation and control algorithms. In Section 6, the DT of MG and physical MG are explained fully with an experimental setup for power and data flow lines. The results for the evaluated DT characteristics are then exhibited. Results provide performance matrices for real-time operation and control, as well as address uncertainty. Lastly, in Section 7 the large-scale proposal is discussed.

2. Background

The existing MG uses control strategies based on SCADA or DCS, and the digital twin system decreases the dependability of these subsystems. However, this [19] paper describes a decentralized MG hosted on the cloud edge. Also, a microgrid security framework is presented in the paper [20], which includes IoT-based web security for MGDT online data. Furthermore, a framework test case is used to improve discrete grid behavior through DT, considering DERs integration issues and frequency synchronization [21]. A respective digital twin-based P2P energy trading is presented in this [22] work. In addition, the MG power dissipation challenge is addressed in this [1,23] work. Here, DT data processing from complex decentralized bus systems is addressed for MG scheduling for optimal ESS management [2] and distribution. In electric grid research, DT are currently flourishing and exploring various sectors of energy management and grid control systems. For instance, the study [24] focuses solely on demand response modeling of microgrids with renewables. Machine learning and AI models have recently been widely used for optimization in the microgrid context. For example, the work [25] centers on cost minimization in energy sharing as prices fluctuate over time, employing a prediction model of costs using real-time data. This [26] research provides a detailed examination of prediction AI and ML models, showcasing comparative performances of AI models in generation forecasts. Similarly, the study [27] presents power management strategies for buildings. Another work [28] utilizes a digital twin approach for battery energy storage system (BESS) capacity estimation. The research [29] focuses on short-term load forecasting, while this [30] study explores deep learning methods for market load prediction in the context of peer-to-peer (P2P) energy trading. These studies indicate that digital twins are being widely used in microgrids, covering specific areas of energy management, power estimation, and control. However, the complete framework is projected to be costly due to the numerous nodes and data involved in developing a comprehensive microgrid digital twin framework. Therefore, an optimized framework is still in order which is done in current work. Table 1 compares related works in the context of digital twin standardization.

Table 1
Recent works comparison on implementation of the digital twin technology in power systems.

Author (year)	Digital model (DM)	Model type	DERs model integration	DT based control	Self-healing DTMG	Optimization
Park et al. 2020 [1]	✗	Optimal ESS scheduling	✗	✓	✗	✓
Zhou et al. (2019) [13]	✗	Network model	✗	✓	✗	✗
Jiang, Zongmin, et al. 2022 [14]	✓	Digital twin body	✗	✗	✗	✗
Saad, Ahmed, et al. 2023 [17]	✗	ES predictive model	✗	✓	✗	✓
Han, Jiaxuan, et al. [19]	✗	Transfer function	✓	✓	✗	✓
Danilczyk et al. 2019 [20]	✗	Web security	✗	✗	✗	✗
Kim, Changhyun, et al. 2022 [21]	✓	Output prediction	✗	✗	✗	✗
Current work	✓	ML-based predictive models	✓	✓	✓	✓

3. Framework modeling

Nowadays, microgrids operate in conjunction with the main grid, facilitating energy exchange during periods of internal demand and surplus production [31]. Key factors in this process include the charge level of the BESS, generation, and load demand. Traditionally, these models are represented discretely and integrated into software or simulation environments for comprehensive system analysis [32]. The power output from the solar panel (P_{pv}) can be modeled as:

$$P_{pv}(t) = \eta_{pv} \cdot A_{pv} \cdot I(t) \cdot \left(1 - \alpha_T \cdot (T(t) - T_{\mathrm{rf}})\right) \tag{1}$$

$$P_{wt}(t) = \frac{1}{2} \cdot \rho \cdot A_{wt} \cdot v(t)^3 \cdot C_p(\lambda, \beta) \tag{2}$$

At a particular time, t, the solar power generation $P_{pv}(t)$ is determined by the panel efficiency η_{pv}, area A_{pv}, irradiance $I(t)$, and temperature coefficient α_T. Similarly, the inputs for the wind turbine generation model include air density ρ, swept area A_{wt}, wind speed $v(t)$, and power coefficient $C_p(\alpha, \beta)$. For a BESS with power capacity E_m, the state of charge (SoC) can be defined as (3), where η_{ch} and η_{dch} are the charging and discharging coefficients, respectively. The terms $P_{ch}(t)$ and $P_{dch}(t)$ represent the charging and discharging power at time t, respectively, while $d_{ch}(t)$ and $d_{dch}(t)$ are the binary decision variables indicating whether charging or discharging occurs. In (5), $P^B(t)$ calculates the net power of the battery at time t. It is the difference between the discharging power $P^B_{dch}(t)$ and the charging power $P^B_{ch}(t)$. The binary decision variables $d_{ch}(t)$ and $d_{dch}(t)$ determine whether the battery is charging or discharging at time t. In this dynamic system, islanding dispatch control depends on generation and demand, with P_{grid} representing the power input to or output from the grid connection terminal to the MG unit. This parameter can be negative when energy is acquired by the MG and positive when energy is discharged to the utility grid. Here (6) represents the dynamic power balance in an islanded microgrid, where $P_{\mathrm{gen}}(t)$ is the total power generated, $P^B(t)$ is the net power flow from or to storage systems (influenced by SoC), and $P_{\mathrm{loss}}(t)$ accounts for system losses. The term $\Delta P(t)$ represents any power imbalance at time t, which must be minimized to maintain system stability. The SoC of storage systems determines their ability to either discharge power into the microgrid or absorb excess power, playing a crucial role in maintaining this balance.

$$SoC(t) = SoC(t-1) + \frac{\eta_{ch} \cdot P_{ch}(t) \cdot d_{ch}(t) - \frac{P_{dch}(t) \cdot d_{dch}(t)}{\eta_{dch}}}{E_m}$$
$$\forall \quad d_{ch}(t) + d_{dch}(t) \leq 1 \tag{3}$$

$$P^B(t) = P^B_{dch}(t) \cdot d_{dch}(t) - P^B_{ch}(t) \cdot d_{ch}(t) \tag{4}$$

$$P_{pv}(t) + P_{wt}(t) + P^B(t) - P_{ld}(t) = P_{grid}(t) \tag{5}$$

$$P_{\mathrm{gen}}(t) + P^B(t) = P_{\mathrm{ld}}(t) + P_{\mathrm{loss}}(t) + \Delta P(t) \tag{6}$$

During the modeling phase, various inputs and outputs must be identified for analysis. In this work, the modeling focuses on maximizing renewable energy generation while minimizing computational cost.

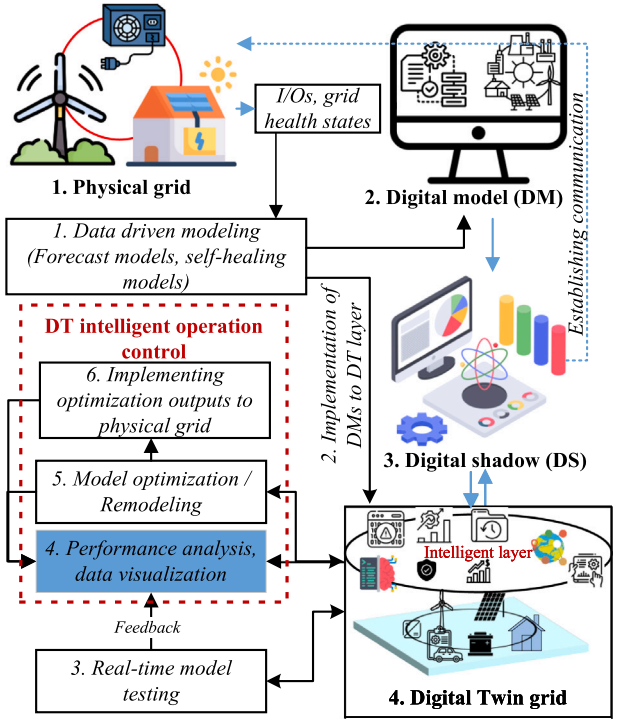

Fig. 1. Development framework for digital twin microgrids with key functional blocks.

This entire process is influenced by different input variables, making dynamic maintenance and processing for networks with multiple generation sources $P_{\mathrm{res}}(t)$ and load components complex and computationally intensive, particularly given the real-time analysis capabilities of digital twin technology.

$$P_{res}(t) = \sum_{i=1}^{n} \sum_{j=1}^{m} \left(P^{pv}_{ij}(t) + P^{wt}_{ij}(t) \right) \tag{7}$$

$$\max \dot{Q} = P_{res}(t) + W_i \cdot C_c(t) \tag{8}$$

Eq. (7) represents the integrated power generation from various renewable energy sources across multiple microgrids. Here, i denotes the microgrid number, and j represents the specific component (PVs, WTs, etc.) within the ith microgrid. The equation sums the contributions from all renewable components across all microgrids. It is important to note that the indices i and j do not imply that the number of PV panels and wind turbines is the same across all microgrids; instead, they reflect the summation across all components within each microgrid. In a cloud database, specific data can be accessed using the ij identifier from the replicated topology configuration.

To optimize the modeling process, the computational cost $C_c(t)$ must be considered to ensure practical implementation. The objective function $\dot{Q}$ in Eq. (8) aims to balance the renewable energy generation model with the associated computational costs. Here, W_i denotes the weight associated with the computational cost of the

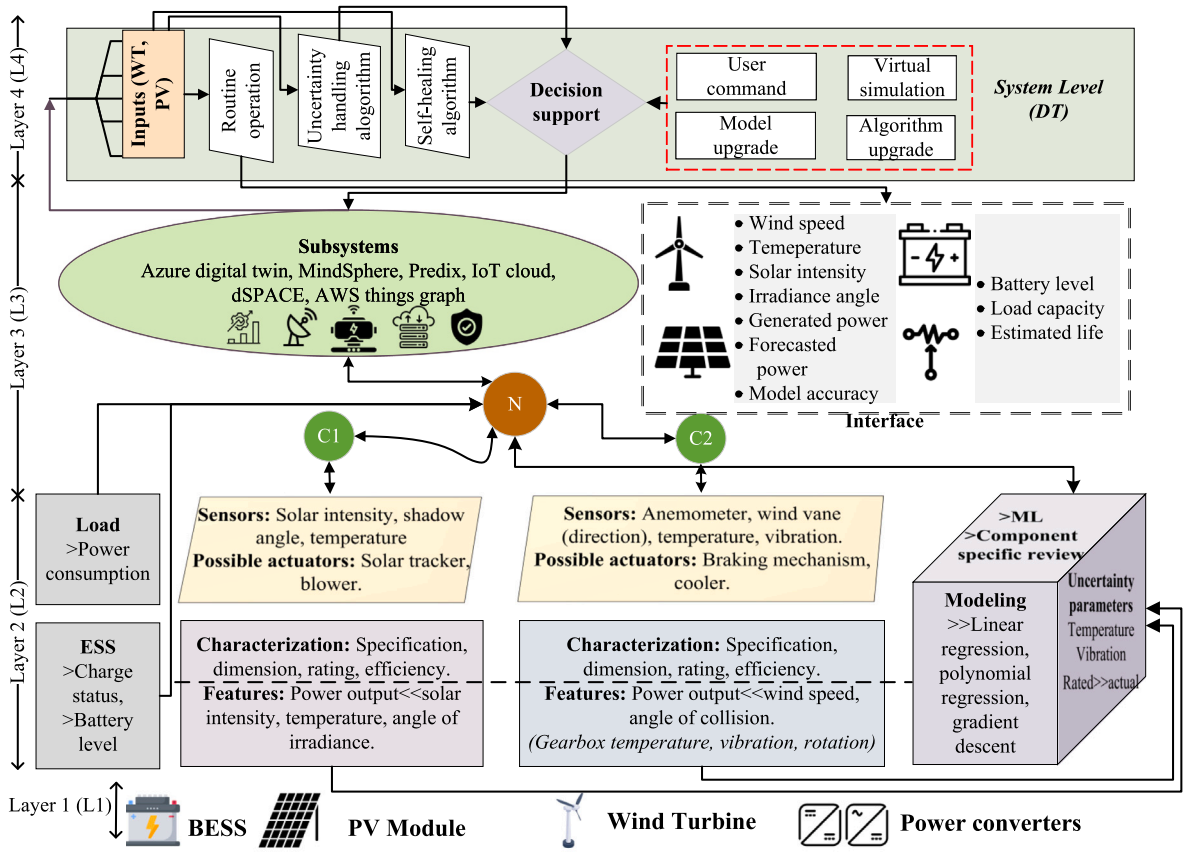

Fig. 2. Implementation of a hierarchical structure of digital twin microgrid.

ith microgrid. Since (8) has both generation and computational cost items, it ensures that the optimization considers both energy generation and computational efficiency. To meet these objectives, data-driven machine learning models will be utilized due to their dynamic nature, ease of development, and computational efficiency [33].

3.1. Digital twins: Development procedure

A digital twin framework mirrors the physical system, encompassing its inputs, outputs, and actions. This framework is deployed in cloud-based online systems and ensures ongoing communication with the physical system [34]. The real-time data processed by the cloud layer serves various functions, including optimization and self-healing [16, 35]. For microgrids, such a system is shown in Fig. 1 which has different levels of functionality. A sensor and instrumentation layer processes data from the physical grid layer. These sensory data are kept in a local storage unit and sent through communication channels to a cloud layer. Data from the cloud layer is received by the final DT layer, which processes it for usage in further operations. The procedures continually maintain the physical and twin layers in bidirectional communication. Reliability and management while using the current cloud infrastructure to follow the platforms' security and communication routes [36].

As shown in Fig. 1, the initial step in developing a digital twin (DT) system is to create a digital model (DM). A digital model can be either a traditional physics-based model or a data-driven model. These models represent the system's variables, which vary based on the specific purpose of the modeling. The digital models (DMs) are then linked to the physical system—in this case, the physical microgrid—forming what is known as a digital shadow (DS). This digital shadow enables communication with the physical system. Finally, an intelligent layer is integrated with the digital shadow to complete the DT framework for a specific system [37]. This intelligent layer makes informed decisions for the management and optimization of the system, elevating it beyond traditional simulation-based systems and representing a digital twin system.

3.2. Data-driven system modeling

The approach adopted in this study is illustrated in Fig. 1. Initially, inputs and outputs of the grid components, such as solar intensity, wind speed, and other input states essential for grid self-healing, are collected. According to the digital twin development scheme, DMs must be created using data-driven methods, and these models are directly stored in the digital twin layer. During the communication phase, physical shadowing is established through bidirectional communication, synchronizing the model variables in the twin layer with the physical grid. The variables are then consolidated into a single gateway, and the data matrix is separated in the cloud layer.

In data-driven modeling, the relationship between inputs and outputs is established through a modeling method, such as machine learning. Under ideal conditions, the modeling of a wind turbine and PV module can be performed using Eqs. (1) and (2). Generally, this relationship is represented as $\gamma^i_{dr} = f(\lambda^i_{dr})$, where γ^i_{dr} denotes unoptimized outputs corresponding to unoptimized inputs, λ^i_{dr}. The term "unoptimized parameters" refers to ideal parameters because the digital twin (DT) modeling is conducted at the current lifecycle stage of the components, reflecting deviations from their rated performance. Consequently, for optimized modeling, the primary input components that can be used to map the output powers of renewable energy generation components are selected. This can be generally represented as $\Gamma^i_{out} = f(\Lambda^i_{in})$, where Γ^i_{out} represents the real-time outputs for the real-time inputs Λ^i_{in}. These digital models are designed to model power outputs and inputs, such as solar intensity, wind speed, etc. Additionally,

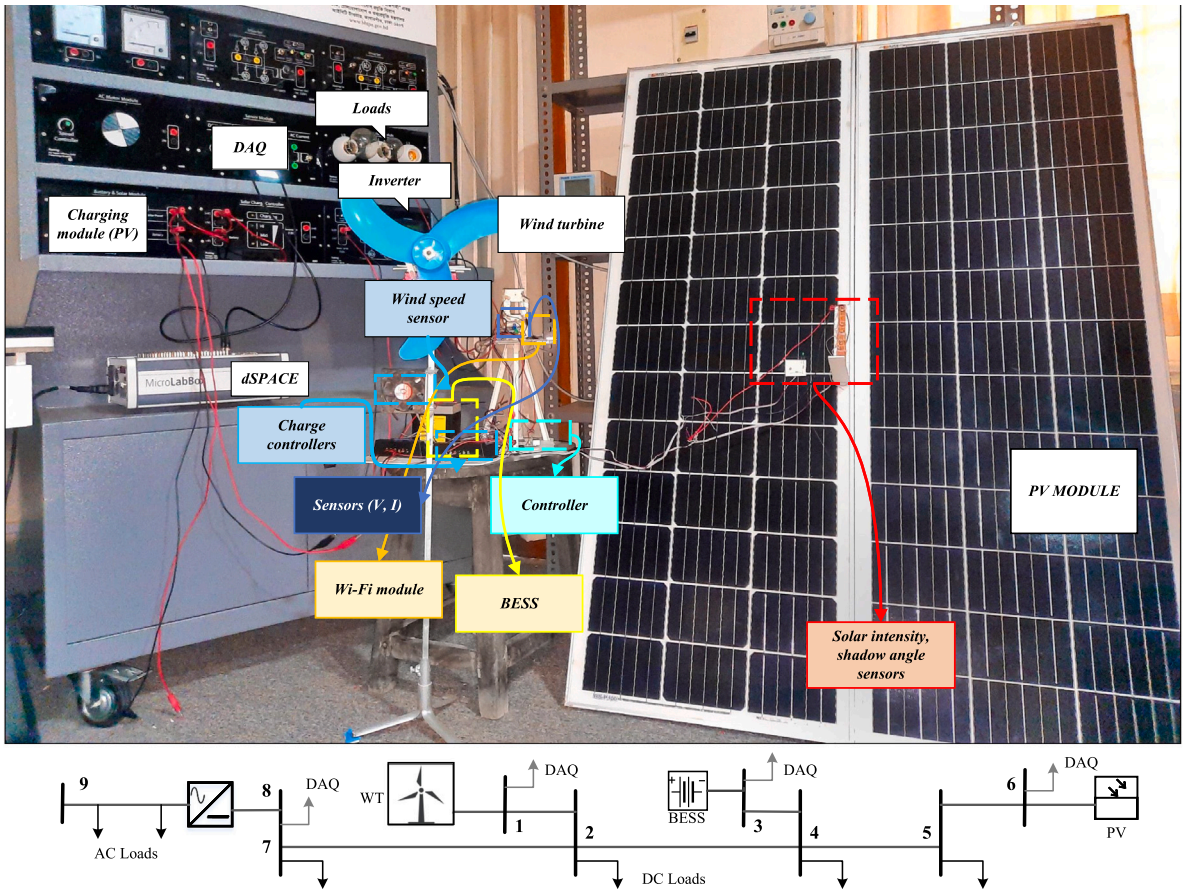

Fig. 3. Overall setup for data acquisition, operation, and control test-bed.

another model for the self-healing system of the microgrid is presented in this work, which can be expressed as $Y^i_{sts} = f(\zeta^i_{dr})$, where Y^i_{sts} denotes the actuation outputs for grid health input states ζ^i_{dr}.

The modeling methodology is outlined in Fig. 1. Initially, the electronics necessary for bidirectional communication of the digital twin are set up, establishing the sensor, actuator, and control network. Next, real-time grid inputs are collected from the sensors for data-driven modeling. Once the modeling is completed, the models are implemented in the digital twin cloud database, where they are dynamically tested, and their performance is visualized using real-time data. Following analysis, the models are optimized to achieve maximum output power from renewable energy sources. The optimized parameters are then applied to the physical grid, and performance is continuously monitored and analyzed to determine if any remodeling is necessary or if there is a need to integrate new models or modify the existing codes. These functionalities are part of the digital twin's intelligent operation control program. This process results in the creation of final models of renewables and self-healing mechanisms for establishing digital twins.

Fig. 2 conceptually illustrates a microgrid node (N) with a PV module and wind turbine, modeled and controlled according to various layer activities. It depicts different function blocks and subsystems of the digital twin microgrid. The MG generation components (C1, C2) state from L1 are projected towards the modeling layer (L2). This layer is divided into two types based on digital twin functions. The first type involves parameters extracted solely for data visualization, such as battery charge level and real-time load information. The second type is directly connected with the digital modeling of components and data synchronization after being modeled, which interacts with the models to display dynamic outputs like predicted power generation or self-healing triggering sequences. In this context, the specified DT modeling of the MG extracts input parameters as features $(\lambda^i_{dr}, \zeta^i_{dr})$. This feature layer extracts load, ESS, and DER data for DT modeling. The parameter-aided model forms the DT layer (L4), supported by operation and grid management algorithms. The twin layer communicates with the cloud and interface layer (L3), functioning as an HMI and data processing unit. L3 and L4 are crucial function blocks for digital twin development. L4 is a virtual cloud layer where programming and data handling algorithms operate in real time, and it is also the place for model updates or other supervisory actions. This layer is quantitatively supported by L3, which limits the work procedure based on the subsystems' characteristics. These subsystems (e.g., Microsoft Azure, and Amazon Web Services) provide storage and the interface for synchronizing physical variables with digital twin model variables. Hence, this layer will also be responsible for factors such as scalability and security.

In the current research, computational cost, component's life-cycle, and scalability are our primary design considerations. To address these, we employ a low-cost data-driven modeling approach for the grid components, which ensures scalability due to its cost-effectiveness. Consequently, the objective function is to achieve sufficient accuracy with these design considerations in mind.

4. Digital twin framework implementation

To establish the modeling concept shown in Fig. 2, an MG experimental setup is employed in Fig. 3 and the data acquisition system for the setup is shown in Fig. 4. In this configuration, a microgrid unit is taken from the distribution bus system that includes renewable energy resources such as a wind turbine and a PV module. The charge controllers and load are coupled to these energy sources. Charge controllers establish a particular node connection between energy sources and

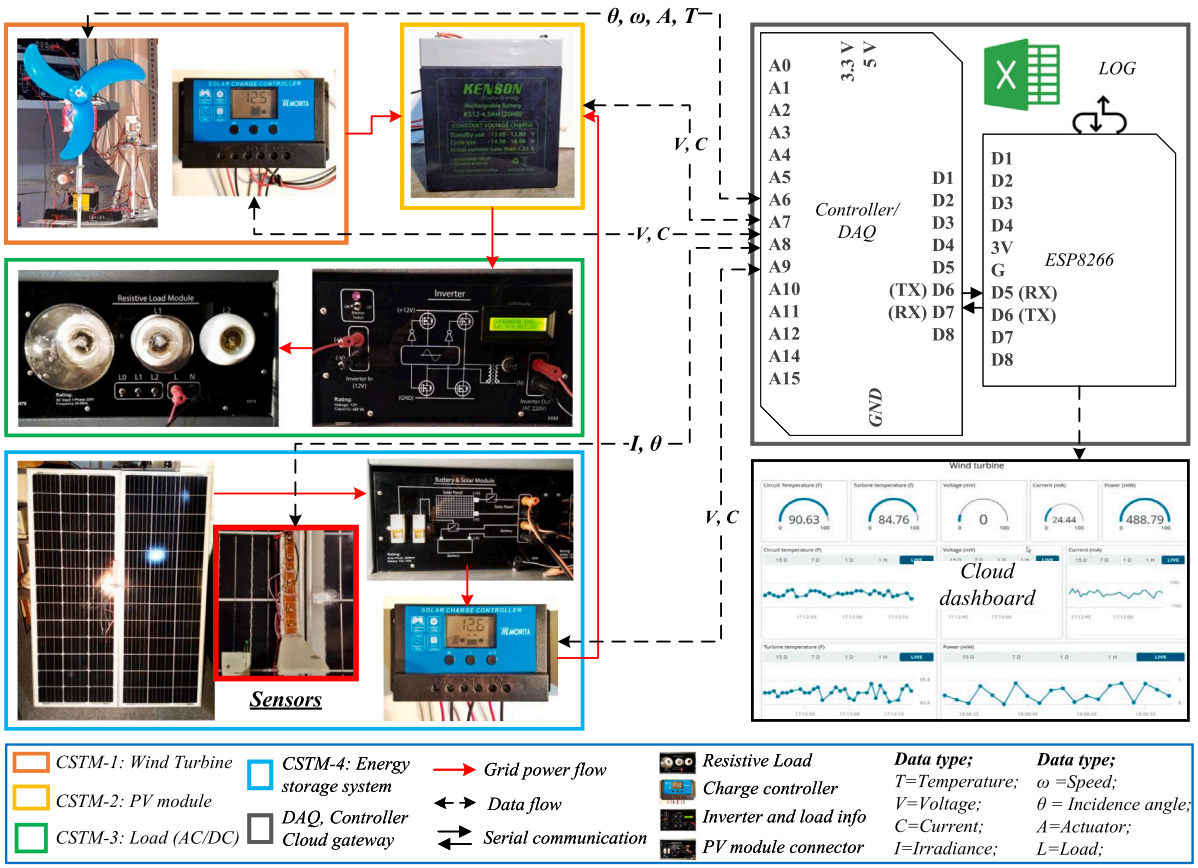

Fig. 4. Communication diagram of the experimental test-bed featuring data acquisition system and flow of power and data.

energy storage systems, resulting in a charging load for the resources. Additionally, each renewable energy source's and load's terminals are connected to the sensors for real-time data collection. The sensor terminals' power information is utilized to duplicate the data display for any change in those terminals. Controllers and a Wi-Fi module are used by dSPACE to handle data from the MG buses before sending it to the cloud. The module acts as a bidirectional data gateway between physical MG and twin MG. Here, I/O state parameters for DERs are used to update DT parameters. To maintain the system state integrity at its current lifespan, the model for the employed specific subsystems is calibrated for both training and testing objectives.

The microgrid unit utilized in this research, as depicted in Fig. 2, represents the distributed MG within a power system network. Given that these systems are currently operational, traditional I/O models exhibit reduced efficiency due to the lifecycle degradation of existing system components. Consequently, real-time data-driven approaches of DT are more suitable. The model constraints (M_c) are presented in Eq. (9), where M_{lf} denotes the lifecycle parameter of RESs and M_{lt} denotes model linearity. These model constraints must satisfy the objective sub-function $\dot{Q}(C_c(t))$.

$$\dot{Q}(C_c(t)) \longleftarrow M_c = W_1 \cdot M_{lf} + W_2 \cdot M_{lt} \tag{9}$$

However, the I/O relationship of the renewable components is nonlinear, necessitating the selection of nonlinear models for accuracy. Advanced models such as neural networks (NN) and support vector machines (SVM) are computationally expensive compared to regression models like polynomial regression due to the use of kernel functions. In small-scale microgrids for individual component modeling, these methods can be effective, but in large-scale systems, the number of models increases with the number of components, leading to high system management costs. Therefore, to optimize computational costs, a simpler model with satisfactory accuracy is required to be selected. That is why, the polynomial regression algorithm is chosen for this experiment. To optimize the model even more, only principal inputs that significantly impact output performance are chosen. This approach allows for quicker data handling compared to model-driven methods that require extensive system information, making big data handling challenging.

To train the models real-time I/O data from the microgrid is extracted using a sensor-based DAQ system. After extracting the data, modeling algorithms are trained. Once trained, the model performances are tested with real-time data. Upon achieving satisfactory accuracy, the model is deployed to the cloud layer, which handles I/O visualization and performance curves of the real-time model presented in this study. After multiple tests, the model is deployed to the cloud layer, establishing synchronization between the physical grid and the digital twin grid with variable syncing.

The algorithm for grid component modeling begins with training the model using input features for photovoltaic (PV) power generation (χ, $\phi \rightarrow \phi_{rad}$, P^{pv}) and wind turbine power generation (ω, $\theta \rightarrow \theta_{rad}$, P^{wt}). It first calculates the sum of squared errors (SSE) for the training data to measure the discrepancies between actual and predicted power ratios (P^{pv}/P^{wt}). Coefficients (L_i) for the model are computed using the normal equation. The model's fit is assessed by calculating the R-squared value, which compares SSE to the total sum of squares (SST) of the training data. The polynomial regression model for prediction is defined to express the relationship between input features and the power ratios. For each subsequent time step, the model predicts the power ratio using the polynomial equation and evaluates the prediction error by comparing the predicted power ratio to the actual value. Hence, the test errors are the percentage error of actual power and model forecast power. The trained models are rigorously tested for reliability before implementation in the cloud layer.

Table 2
Modeling of PV module with inputs of light intensity and tilt angle.

Intensity (W/m^2)	Angle (degrees)	Temperature (°F)	Power (W)	Coefficients					
				L_0	L_1	L_2	L_3	L_4	L_5
10.44	90	78	1.07	62.42	−202.62	0.00	4.79	63.96	0.0
10.4	90	78	1.13	9.00e+09	−3.8e+11	1.22e−04	1.78e+00	2.44e+11	0.00e+00
10.56	90	78	1.14	0.0	−4.2e+11	−2.3e+11	−3.26e−02	2.68e+11	−9.1e+10
9.72	83	78	1.13	0.0	0.11	0.001	−0.006	−0.001	0.005
8.16	83	78	1.07	0.0	2.40e−02	−6.1e+09	−3.04e−02	3.78e−01	2.01e+09
7.52	83	78	1.07	0.0	0.45	0.10	−0.01	−0.12	0.32
6.8	75	78	0.94	0.0	0.43	1.33	−0.01	−0.10	−0.10
8.76	75	78	0.81	0.0	−2.27e−01	2.37e+01	−2.07e−02	4.25e−01	−9.27e+0
10.28	75	78	0.93	0.0	−1.42e−01	2.32e+01	−8.69e−03	2.21e−01	−8.46e+0
7.4	62	78	0.68	0.0	0.33	1.90	−0.01	−0.01	−0.09
9.16	62	78	0.75	0.0	0.42	−1.89	−0.01	−0.11	1.50
11.08	62	78	0.81	0.0	0.50	−2.34	−0.01	−0.21	1.99

Algorithm 1 Grid component modeling.

1: {Training the model}
2: TRAIN($\chi, \phi \rightarrow \phi_{\mathbf{rad}}, \mathbf{P^{pv}}; \omega, \theta \rightarrow \theta_{\mathbf{rad}}, \mathbf{P^{wt}}$)
3: {Calculate SSE for training data}
4: $SSE = \sum_{i=1}^{n}((P^{pv}/P^{wt})_i - (P^{pv}\hat{/}p^{\hat{w}t})_i)^2$
5: {Compute coefficients $\mathbf{L_i}$ using the normal equation}
6: $\mathbf{L_i} = (\Lambda^T\Lambda)^{-1}\Lambda^T \cdot p^{pv}/p^{wt}$
7: {Calculate R-squared value for the model}
8: $R^2 = 1 - \frac{SSE}{SST}$
9: {Calculate SST for training data}
10: $SST = \sum_{i=1}^{n}((P^{pv}/P^{wt})_i - (P^{pv}\bar{/}p^{\bar{w}t})_i)^2$
11: {Define the polynomial regression model for prediction}
12: $(P^{pv}\hat{)}P^{wt}) = \mathbf{L_0} + \mathbf{L_1}(\chi/\omega) + \mathbf{L_2}(\phi/\theta) + \mathbf{L_3}(\chi/\omega)^2 + \mathbf{L_4}(\phi/\theta)^2 + \mathbf{L_5}(\chi/\omega)(\phi/\theta) + \ldots + \mathbf{L_n}(\chi/\omega)^{m_1}(\phi/\theta)^{m_2}$
13: {Use the model to predict the next time step}
14: **predict** $(P^{pv}/\hat{P}^{wt})^{t++} = \sum_{i=1}^{n} L_i f^{t++}(\chi, \phi, \omega, \theta)$
15: {Calculate prediction error}
16: **error**$(e_t) = 1 - \frac{P_{pre}^{pv/wt}}{P_{act}^{pv/wt}}$

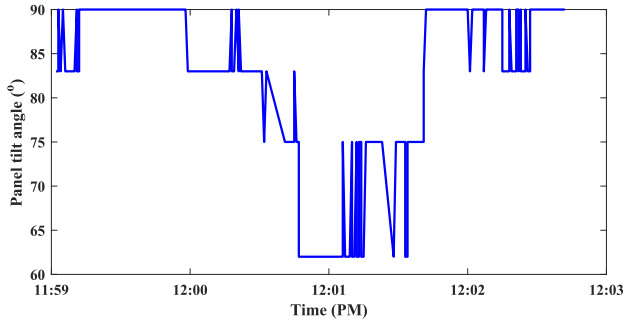

Fig. 5. Panel tilt angle test case for PV module.

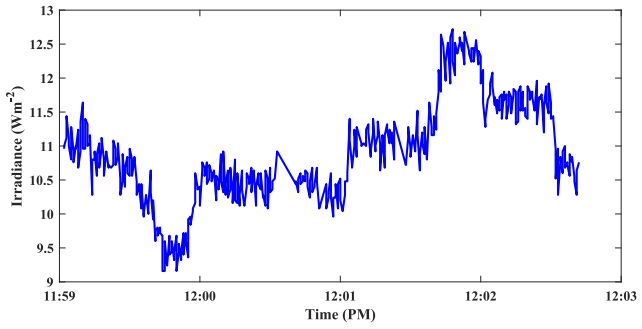

Fig. 6. Solar intensity test data in W m^{-2}.

Table 3
Modeling of a wind turbine with inputs of the incidence angle of air and corresponding speed.

Epoch	Angle (degrees)	Wind velocity (m/s)	Power (mW)	Coefficients		
				L_0	L_1	L_2
3	90	31.41	5055.8	0.	0.	0.
9	90	29.75	5897.6	0.	1986.71	−33.13
10	90	34.6	5276.8	0.	324.47	324.47
29	90	22.38	4613.8	0.	393.03	−6.24
200	90	52.85	8408.4	0.	−274.4	4.95
203	90	57.55	9755.6	0.	−262.6	4.91
249	90	54.22	9755.6	0.	−100.6	3.18
290	90	48.34	8073.6	0.	86.73	0.84
295	90	52.53	10 132.6	0.	99.20	0.69
316	90	48.95	8408.4	0.	176.91	−0.19
331	90	54.6	9422.4	0.	206.99	−0.57

DT model of the PV module takes I/O parameters as $\Lambda_{pv}^t \leftarrow \Psi^t(\chi^t, \phi^t)$ and $P^{pv} \leftarrow I_{out}^{pv}$. Indoor apparatus is utilized in this experiment to alter the solar intensity and angle, generating a distinctive dataset for the mathematical model. Because there was no temperature deviation, the specific characteristic had no bearing on the outcome. As a result, intensity (χ) and angle (ϕ) are used to create the mathematical model for the power flow equation. To obtain the best-fit line for the dataset provided in Table 2, polynomial regression of degree 2 is applied, and an 86% of accuracy is achieved with Algorithm 1. Which performs iterations for fitting output power, $P_n^{pv(t)}$ with input attributes χ_n^t, ϕ_n^t. The final model for the PV module is shown in (11).

$$P_t^{pv}(W) = L_0 + (L_1 + L_4)\cdot\chi_t\cdot\sin\phi_t + (L_2 + L_5)\cdot\sin\phi_t + L_3\cdot\chi_t^2\cdot\sin\phi_t \tag{10}$$

A feature vector (Λ_{pv}^t is formed, and regression aiming P^{pv} is obtained in every state, generating regression coefficients L_i. The polynomial regression model contains linear and quadratic terms of features. From Λ_{pv}^t, a real-time acquired data vector is recorded for the model. Where a degree 2 polynomial produces 5 coefficients for feature matrix Λ and further fitness pushes a bias term (L_0) as (14).

$$P_t^{pv}(W) = 0.35\cdot\chi_t\cdot\sin\phi_t - 0.1\cdot\sin\phi_t - 0.02\cdot\chi_t^2\cdot\sin\phi_t \tag{11}$$

The tilt angle is between 60 and 90 degrees. As indicated in Fig. 5, particular angles are employed for each test instance. Another input parameter $\Lambda_t(\phi)$ for the PV module is the solar intensity profile which is shown in Fig. 6. For the input profiles ($\Lambda_t(\chi, \phi)$) physical grid generation and model-based output prediction are acquired via the DAQ system. Real-time forecasting error for the acquired data is calculated from actual and predicted outputs P_{act}^{pv} and P_{pre}^{pv}. The outputs $\Gamma_t(P_{dt}, P_{act}, e_t)$ are presented in Fig. 7. The average predicted inaccuracy in the test is around 19%. Due to the quick shift in test situations, a minimum of 0% and a maximum of 53% inaccuracy are observed

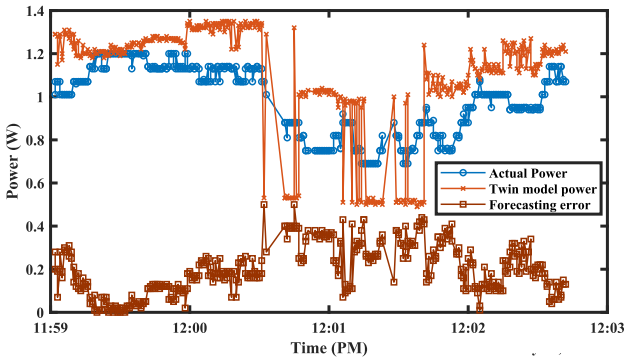

Fig. 7. The test outputs performances: Actual power (W), Model predicted Power (W), and forecasting error.

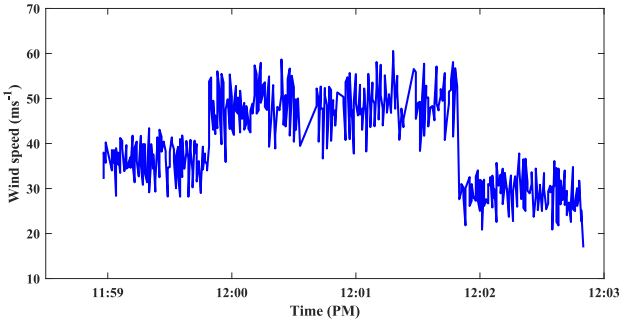

Fig. 8. Real-time wind speed test data in m/s.

throughout the trial. Wind velocity data ω^t is linked with produced power P^{wt} as the I/O conjunction for the wind turbine model. Because the wind always hits the blades vertically when using a weather vane, angle data (θ^t) has no influence on the output equation. However, dynamic wind speed and direction instability cause output fluctuation.

$$P_t^{wt} \gtrless P_{t++}^{wt} \quad \forall \quad \omega_t \approx \omega_{t++} \tag{12}$$

Therefore a moving average approach is utilized in data collection and feature testing to provide a less fluctuating data flow i.e. $|P_t^{wt} \approx P_{t++}^{wt}| \ \forall \ \omega_{t++}$. Regression coefficients for some of the epochs with corresponding I/O's are listed in Table 3. Similarly, as the PV model using Algorithm 1, the model is obtained, which provides a relationship as (14).

$$P_t^{wt}(W) = L_0 + L_1 \cdot \omega_t + L_2 \cdot \omega_t^2 \tag{13}$$

$$P_t^{wt}(W) = 0.00 + 167.36 \cdot \omega_t - 0.28 \cdot \omega_t^2 \tag{14}$$

Test-bed input profile $\Lambda_t(\omega)$ for the wind turbine is shown in Fig. 8. Wind speed is varied at specific and random speed zones. The speed is mapped at an increased profile for sensor sensitivity and efficient modeling. For the input profile with a weather vane output profiles ($\Gamma_t(P^{wt}, e_t)$) are displayed in Fig. 9. For the turbine, an average inaccuracy of roughly 14% is observed. The transition of test cases in the speed profile increases model inaccuracy. In an operation sequence, a continual model error of more than 10%, on the other hand, produces an alarm for a system difficulty.

In order to provide a specific output to the charging load, CSTMs must also be integrated. The real-time integration within the cloud infrastructure is managed by assigning a distinct ID for each variable within a single node and declared in the cloud layer. These physical grid variables are updated through the cloud gateway, maintaining synchronization with the cloud-defined variables. In terms of input

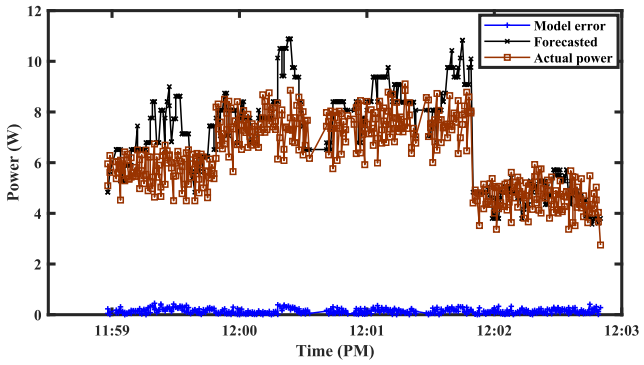

Fig. 9. The test outputs performances: actual power (W), the model predicted Power (W), and forecasting error.

states $\Lambda_{in}(\chi, \phi : \omega)$ and output states $\Gamma_{out}(P^{pv/wt})$, each MG component is referred to as a distinct node (WT_x, PV_x). An integrated model may be accessed via a node ID, and the ID can be used to get all state data for a particular component (WT_1, PV_1). In contrast to model-driven prediction outputs, $P_{pre}^{pv/wt}$, which are generated through input conditions, physical grid-end data, $P_{act}^{pv/wt}$ are immediately updated. Now the integrated system model of a cloud dashboard is a virtual data-based model that shows the status of RESs in real-time as well as how they contribute to the load. The model with manual test cases helps create a digital twin of the microgrid by allowing users to visualize the impact of different input scenarios on the output. Future CSTMs will include more nodes such as (15) and (16) for the specific DERs (P^{PV_n/wt_n}) to address the integration issues with the conventional MG management systems.

$$P^{pv_1} = \Lambda_1(\chi, \phi) \qquad P^{pv_n} = \Lambda_n(\chi, \phi) \tag{15}$$

$$P^{wt_1} = \Lambda_1(\omega) \qquad P^{wt_n} = \Lambda_n(\omega) \tag{16}$$

5. Operation and control methods

The operation and control design of the microgrid in this paper is presented in the context of maintenance strategies against health index and system failure such as overheating. The stability of the proposed technique is guaranteed through energy generation and optimization management with a special consideration of self-healing. When uncertainties threaten a system's routine, the digital twin layer activates necessary sequences to maintain operational stability, especially during physical threats causing heating issues. After addressing these uncertainties, the generation system's performance is automatically restored. Consequently, this method restricts the increase in input voltage and prevents damage that could permanently shut down the system. This autonomous method ensures secure and reliable operations, maintaining continuous operational stability.

A DT microgrid network has CSTMs, and each CSTM has a defined set of states, ζ_{dr}^i. The operational MG will have a performance and stability impacting parameter vector Y_{sts}^i, whilst modeling employs the appropriate I/O ($\Lambda_{in}^i, P_t^{pv/wt}$) characteristics. The characteristics specify failure scenarios as well as the system's capability for shifts, intensity, temperature (T^t) vibration, and other RES-specific factors. For control and routine operational DT refreshes these system and subsystem statuses. Where control and operational methods are used, complete DT replicates particular characteristics. Such state case procedures are defined by Algorithm 2 for operational objectives. Which updates the states and performs predictive maintenance, optimal input tuning, and self-healing procedures.

Traditional microgrid operation entails power generation, storage, and dissipation via DER management and charging modules. Which uses static and command-based or inflexible control operations that

do not push optimal input profiles $\Lambda^{t++}(\chi,\phi,\omega)$. However, with a twin MG, a control approach for maximum power usage is performed dynamically with a gradient descent optimizer as $\nabla_{(\chi,\phi,\omega)} \odot P^{pv/wt}$ as shown in Algorithm 2. Also, the algorithm splits the whole operation routines ($read(in) \rightarrow \Lambda^t(\chi,\phi,\omega)$, $write(out) \rightarrow P^{pv/wt}_{act,pre}$, and calculate error ($e_t$)), subroutines ($log : (\Lambda,\Gamma)_{dr}$), and control actions: read(sts) and write actuations (A^t) as a function of the digital twin MG intelligent layer with logistic regression model. Here, $SW^t_{act/dt}$ is an emergency switch representation of the physical grid and twin grid, and T^t_c is subsystem temperature state data which is simulated as a failure scenario. Accordingly, predicted output $P^{pv/wt}_{pre}$ and actual grid generation $P^{pv/wt}_{act}$ aids in real time model error (e_t) calculation. Logistic regression trained model predicts uncertain events and activates binary-classified uncertainty control techniques. Here, nth activated actuation A^t_n are gained by the binary activation function $\frac{1}{1+e^{-z}}$.

The microgrid in this experiment includes equipment such as DERs, charge controllers, ESS, and loads as shown in Fig. 3. The grid components are incorporated into the physical grid, and a cloud-based responsive model is required for its twin grid. Fig. 3 depicts a system in which a wind turbine and a PV module generate electricity and supply it to renewable charge controllers connected to an ESS and loads. All of these terminal voltages ($V^T_{wt,pv,Ld}$) and currents ($I_{wt,pv,Ld}$) information are going across the data line in a dSPACE DAQ and controller from the sensors. For real-time cloud connectivity, a WiFi chip is utilized. This paper's goal is to demonstrate DT-based control and operation; hence, it was tested under indoor illumination and simulated wind profiles. In such cases, all of the sensors utilized in the experiment are calibrated for this specific environment. For the PV model, solar intensity sensors and shadow detectors are utilized. For the wind turbine model, a wind speed sensor and wind direction features (weather vane) are employed. These sensory data from the charging and discharging sides are supplied to the DAQ and controllers for cloud-based data updates, bilateral operation, and control communications. Physical grid adjustments and DT system-level commands are transmitted through a serial communication link between the controller and the WiFi module. The wind turbine subsystem's temperature is sensed by a thermistor, while the brake system's actuator is a servo mechanism. Any decisions made by either layer will have an impact on P_{act} and e^t, which set the DT for the MG.

Algorithm 2 Grid operation and control.

```
OPERATION
    read, λ^t(χ, ϕ : ω, θ : V_Ld, I_Ld)
    serialwrite : forecast : Log, f^t → P^t_dr : P^t_Ld : e_t
MAXIMIZE(P^pv/wt)
    ∇ · P^pv/wt = (∂P^pv/wt/∂(χ/ω) = 0, ∂P^pv/wt/∂(ϕ/θ) = 0)
    update (χ, ϕ : ω, θ)^t++ ← (χ, ϕ : ω, θ)_optimal

CONTROL
    read  ζ(SW^t_m:c, T^t_c, ω^t, e_t)
    Out ⟵ A^t_n  ∀  ζ_0−n
    X ← Features matrix [ζ(SW^t_m:c, T^t_c, ω^t, e_t)]
    Θ ← logistic regression model parameters
    z ← X · Θ^T {Weighted sum}
    h(X) ← 1/(1+e^−z)
A^t_n ← argmax(h(X)) {Highest probability (out)}
if A^t_n ⟵ predictive maintenance  ∀  ζ^t_i
then A^t_0 → A^t++_1 → safemode; uncertainty
end if
return A^t_n
```

5.1. Data flow

DT approaches big data as a future technology that depicts the system as accurately as possible. The key concept for such a system is IIoT-based data management and control, which combines it with a cyber–physical system (CPS) principle [38]. All device data is archived and processed on a cloud layer in these systems, and a sensor network is required to upload the data into an organized and secure cloud platform. The sensors collect data, and the raw data is analyzed and calibrated with an ML algorithm to provide the highest possible accuracy to the DT model. The concluding interaction occurs between the modeled subsystems and data sent from the physical MG to the IoT-based virtual grid. Fig. 3 illustrates such data flow buses with dotted lines. These are input data that get handled using the existing cloud standards. These lines also carry outputs, and both handling algorithms work in real-time, as demonstrated in algorithm 2. Real-time processing aids in decision-making under uncertain circumstances and in autonomous service routines. In Algorithm 2, the phrases robustness, safety, and security (RSS) are combined into a single term to describe uncertainty measures and equivalent automated actions required from the controlling IoT layer for self-healing or producing alarms as well [39]. The data flow part is an operational section that reads real-time data from PV modules as $\chi^t \leftarrow \chi^{t++} : \phi^t \leftarrow \phi^{t++}$ and wind turbine as $\omega^t \leftarrow \omega^{t++}$), and dc loads ($V^t_{Ld} \leftarrow V^{t++}_{Ld} : I^t_{Ld} \leftarrow I^{t++}_{Ld}$. These real-time data are critical for recognizing events, performing predictive maintenance, and storing the device's lifecycle performance index.

5.2. Power flow

Fig. 3 depicts the power flow of the DERs and other microgrid components. Energy from the sources is routed through charge controllers, which filter and convert an input signal to grid frequency, and the charge controller's output is connected to the ESS, DC loads, and inverters for managing AC loads. The main power bus is supplied by two generation sources (PV, WT) and is connected to inverters, the battery, and DC loads. However, because the grid is linked to its digital twin, all power flow data is exchanged in real time through data flow buses. Any power outage or grid-specific behavior may be determined using specific data, as this increases forecasting error e_t. In uncertain situations or through digital twin commands, the traditional power flow can be disrupted, highlighting the autonomous and supervisory control capabilities of the digital twin's intelligent layer. When the discrepancy between projected and real power surpasses a certain level, the related actuation $(A^t)_n$ mechanism (braking) activates to investigate a specific issue in the specific grid components (e.g. turbine). The power flow operates in a conventional way, with generation components supplying the energy storage system (ESS) and loads, and the battery discharging to compensate for any shortages on the main bus. However, real-time twin grid monitoring assists the controller in managing real-time power variations and breakdowns at various terminals of the MG.

5.3. Generation optimization

In this case, optimization plays a crucial role in selecting input values that maximize performance, aligning closely with the parameters of interest. The algorithm utilizes a methodical approach where the first partial derivatives are calculated to emphasize specific attributes, such as $\frac{\partial P^{pv}}{\partial(\chi/\phi)}$ for photovoltaic power and $\frac{\partial P^{wt}}{\partial(\omega)}$ for wind turbine power. These derivatives guide the search for optimal input conditions that enhance the outputs of DERs. The optimization process involves setting up conditions $\Lambda'(\chi,\phi) = 0$ and $\Lambda'(\omega) = 0$ to determine state solutions that yield maximum outputs. By iteratively adjusting input parameters based on these derivative-guided optimizations, the algorithm aims to achieve peak performance in energy generation from photovoltaic and wind sources. This method utilizes the developed digital models, eliminating the need for additional data acquisition to achieve optimized inputs and outputs.

5.4. Control strategies

This work emphasizes digital twin specialized intelligent control systems for managing uncertainty, self-healing, and routine operations in external subsystems like sensors and actuators, all within the DT framework. The developed model guides output behavior by establishing twin phenomena, aiming to manage grid asset uncertainties and control specific grid states through parameter synchronization with the DT layer. On the other hand, the control strategy of a DT-based system is a combination of autonomous, supervisory, and uncertainty control, which is assured by the real-time bilateral communication feature of DT, resulting in self-healing and status monitoring. This involves autonomous feedback-based management of optimized input parameters while addressing uncertainty. Consequently, the current control focuses exclusively on the specialized sensor and actuator configurations necessary for digital twin development. The goal is to maintain operational stability while maximizing output from the generation components. The traditional grid control systems for regulation and conversion remain operational, while an external sensor, actuator, and controller arrangement has been implemented to manipulate grid health states and generation component inputs. This setup quantifies the applicability and capability of the digital twin in the MG.

5.4.1. Autonomous control

The applications and research of digital twin technology are extensively conducted in industrial automation and processes more than in any other sector. The principles of Industry 4.0 align perfectly with the novel digital twin technology, supporting the establishment of DT focused on the autonomous control of grid natural operations. In this context, autonomous control actions are executed for self-healing and to test the performance of the developed subsystems. Autonomous control systems enable optimal operation of the system, even in scenarios where failures are possible. For self-healing, first, the threshold values from the grid component's system behavioral research are stored as $T_{th}, \omega_{th}, e_{th}$. Every second, real-time sensory data (T_c^t, ω^t, e_t) are refreshed and compared to these thresholds. For a wind turbine, if the values exceed the thresholds, it may cause resonance in the gearbox, yaw drive, or blades. As a complete brake in a high-speed wind condition raises pressure at the tower's tip, such a scenario necessitates breaking $(A_0^t \rightarrow A_1^{t++})$ at a fuzzy level respecting wind speed. Another test feature is the temperature of the power converter and gearbox. When these readings exceed the threshold, the control action activates the brake and active cooling mechanisms $(A_0^t \rightarrow A_1^{t++})$. After mitigating such events the process is restored automatically. This is how the twin grid ensures self-healing control while also keeping the alerts and activities recorded for future reference and predictive maintenance. The results section displays the output behaviors for these autonomous management operations.

5.4.2. Supervisory control

Supervisory control actions are initiated from the digital twin layer during emergency situations or when there is a need for command modifications, system remodeling, or reprogramming. The taken actions gets updated in both physical and twin grid at the same time because each of the physical grid input states (ζ_i) is linked with a corresponding set of variables in the DT cloud layer. Synchronization between these two layers allows for downloading and uploading changes made in either layer. To facilitate data integration, models are created to ensure data exchange occurs efficiently, reducing computational complexity. Supervisory actions can override autonomous control actions, thereby limiting changes that could lead to unstable operations. In this experiment, supervisory control served as a flag master switch (SW_{act}^t) operations. While this is operated, the entire grid operation changes its states accordingly, and a similar action may be initiated by the cloud platform (SW_{dt}^t) as well. Besides managing data and supervisory operations, the cloud layer handles reprogramming, remodeling, and algorithm performance testing. In these scenarios, reprogrammed actions are evaluated using real-time data to assess the effectiveness of the adopted method for the specific system. Reprogramming actions and virtual simulation models do not function as a digital twin model until the model variables are synchronized with the physical variables. This approach provides an opportunity for beta testing and evaluating control actions before implementing them in the physical system. In this research, such pre- and post-implementation actions are undertaken to enhance the system's operational reliability, stability, and model accuracy.

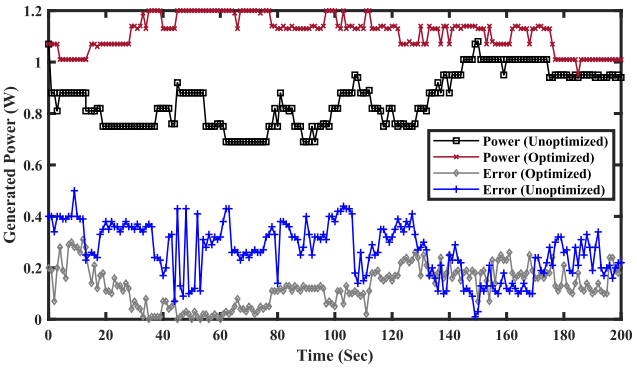

Fig. 10. Optimized and unoptimized output power for the solar panel.

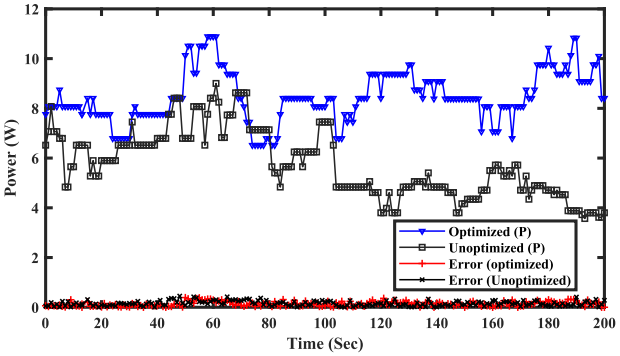

Fig. 11. Optimized and unoptimized output power for the wind turbine.

6. Results

The method of gradient descent is applied to the digital models to maximize the output of the corresponding models by pushing the optimal profiles χ_{opt} and ϕ_{opt}. The optimized input–output profiles for the PV module and wind turbine are presented in (17) and (18) respectively. Additionally, the optimization of CSTMs identifies the profiles that maximize output within the trained model. Since the solar intensity and wind speed are natural states, the optimization of the grid level takes place with optimal values of the tilt angles (ϕ_{opt}, θ_c) of the solar panel. The resulting output power is shown in Fig. 10. Similarly, for the wind turbine, the optimized outputs are presented in Fig. 11. The unoptimized data is subject to varying inputs in a random manner, whereas the optimized profile is specifically adjusted to the wind turbine setup to capture the maximum power in that particular environment. In this context, the digital twin's predictive maintenance plays a crucial role by proactively managing the turbine to achieve optimized output. This underscores the success in attaining maximum power efficiency and ideal state configurations through predictive analysis applied during experimentation.

$$P_{max}^{pv} = 1.50 \;\; W\chi_{opt} = 12 \;\; \mathrm{W\,m^{-2}} \qquad \phi_{opt} \approx 90^{\circ} \tag{17}$$

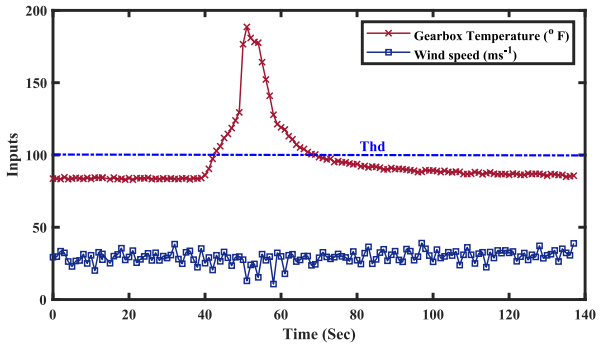

Fig. 12. Temperature test input for turbine gearbox.

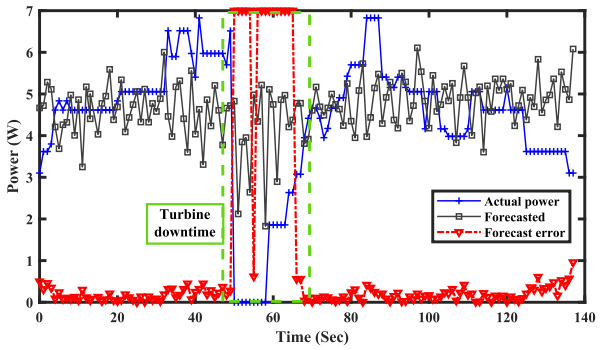

Fig. 13. The self-healing test output performance in response to the gearbox temperature: actual power (W), the model's predicted power (W), and forecasting error.

$$P_{max}^{wt} = 10.76 \;\; W\omega_{opt} = 60.56 \;\; \text{m s}^{-1} \qquad \theta_c = 90° \tag{18}$$

The self-healing control in this work focuses on extreme grid health states that could lead to hardware failures. The proposed self-healing technique is designed in terms of tackling physical system failures such as overheating. For real-time self-healing of MG management, turbine temperature is selected as a supporting state parameter Y_T. Figs. 12 and 13 depict a self-healing test case in which an infinite error in the power model was noticed at the moment of gearbox temperature rise. Because the physical grid power is 0 in this case, its error is infinite. However DT model operates by initiating a control sequence of actuation. The turbine brake mechanism is triggered as soon as the temperature starts going over a safety threshold (thd). When the temperature fell below the threshold for self-healing action and uncertainty handling algorithms, the turbine resumed operation. Uncertainty parameters do not have to be limited to gearbox temperature; they might also include vibration, speed, or a fuzzy mix of more than one parameter for a certain CSTM. One of these instances of cloud-based action updating and a digital twin bidirectional data flow approach is shown in Fig. 13. The self-healing control system activates a turbine braking mechanism and manages temperature rise, with an average response time of 1.2 s. The service restoration time was around 30 s, demonstrating high effectiveness in the experimental setting.

The present work introduces a data-driven technique for creating a digital twin for microgrids using real-time data analytics to optimize generation and enable self-healing. This approach improves upon traditional static models [40] by offering more responsive strategies. While model-driven methods require extensive prior system information [41], the current method hence data-driven modeling only needs system I/O information, simplifying the development of DTs with many components. This work not only proposes the way for large-scale applications but also advances microgrid modeling and operation with DT-based practical solutions. Unlike traditional methods like geographic surveys for generation optimization [42], our approach achieves optimization directly from the model. While optimization in classical methods requires extensive model information and may still be inapplicable due to lifecycle degradation at the time of application. The gradient-driven method used in this research only require the model to be optimized with data from components' current operational lifecycles. This approach results in more accurate models and reliable optimized parameters. Additionally, it emphasizes self-healing control to maintain operational stability and address physical failures, areas often overlooked in recent research [43]. In recent works, self-healing terms are widely explored in terms of cyber security [44] and service restoration in the events of cyber attack however grid physical health parameter self-healing with the complete DT framework is presented here.

However, this study validates the establishment of DT in a microgrid setting. The configurations and subsystems used in this research are based on existing technologies. The performance parameters and device configurations are presented in Table 4, where the communication latency is shown to quantify the system's operational and communication speeds. From the table, it can be observed that the average data acquisition cycle was approximately 1 s, creating datasets for around 10 min of data. This table also provides information about the scalability of the current research. The model size and system configurations indicate the full scalability of this approach. The scalability factor also depends on the subsystem configuration and data processing speed, such as cloud databases [45], which limits the number of variable management and model sizes, thereby indicating the system's wide scalability opportunities.

7. Large scale proposal

This research focuses on building a digital twin model for a microgrid, which can be scaled up to represent larger power systems containing multiple microgrids and traditional grid elements. To achieve this, the study utilizes cost-effective modeling techniques that can handle large-scale implementations. The same modeling approach can be applied to individual grid components within a larger system. After creating these models, they all need to be integrated into a cloud-based system to manage the real-time behavior of the physical power system.

In Fig. 14, the visualization depicts a grid bus system with several generation and distribution elements. That incorporates renewable energy sources (WT_x, PV_x), energy storage systems (ES_x), and sensory networks. The bus system also includes diesel generators (G_1-G_3) and the conventional utility grid. For distributed generation and flexible operating modes, transformers, and inverters are used in the physical grid. The sensory network encompasses the terminal points of these devices. Terminal data provides information about the system's I/Os, which will be used to construct models.

For large scale systems the model will be integrated in a data matrix with a unique ID to access the particular unit. This research uses only principal components through and the limited variables ensures sustainability for the larger network. For this, the network can be represented as follows:

$$P_{WT_k}(\omega) = a_k\omega^n + b_k\omega^{n-1} + \cdots + z_k \tag{19}$$

$$P_{PV_m}(\chi) = c_m\chi^n + d_m\chi^{n-1} + \cdots + w_m \tag{20}$$

$$P_{MG} = \sum_{k=1}^{i} P_{WT_k}(\omega) + \sum_{m=1}^{j} P_{PV_m}(\chi) \tag{21}$$

$$P_{total} = \sum_{MG=1}^{n} P_{MG} \tag{22}$$

$$P_{total} = \sum_{MG=1}^{n} \left(\sum_{k=1}^{i} P_{WT_k}(\omega) + \sum_{m=1}^{j} P_{PV_m}(\chi) \right)_{MG} \tag{23}$$

The above equations represent the combined polynomial regression models for WT and PV modules across multiple distributed MG. The

Table 4
The performance parameters of the used devices.

Sl.	Entity	Configurations	Delay types	Delay
1	Controller	Frequency: 16 MHz, Memory (max): 256 kB	Latency	10 ms
2	ESP8266 (WIFI module)	Frequency: 80 MHz, Memory (max): 4 MB, Upload rate: 1 Mbps	Latency	50 ms
3	Sensors	Error: ±1%	Detection delay	30 ms
4	Controller	Adjustable	Stabilization + serial communication	850 ms

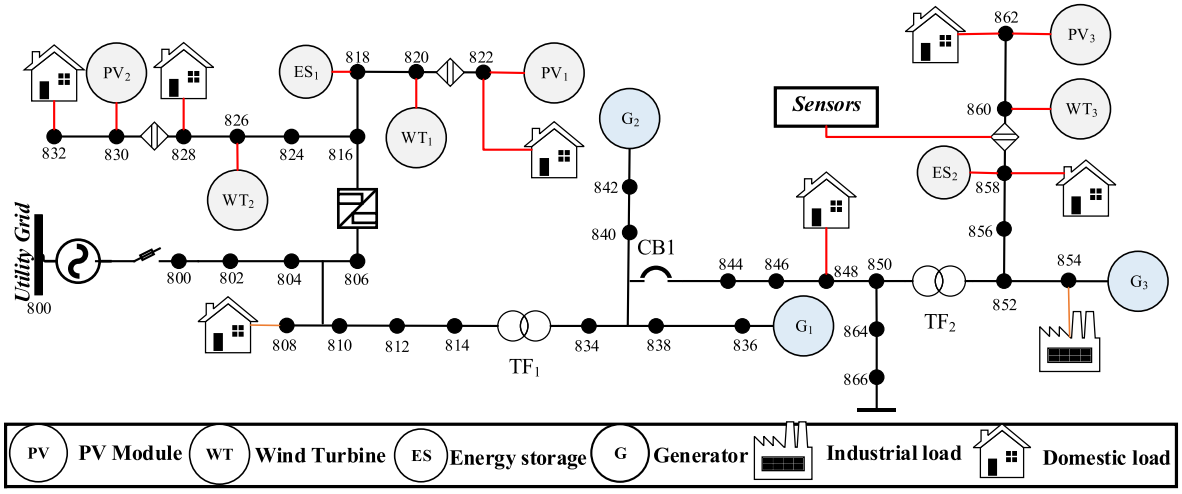

Fig. 14. Large scale DT framework implementation with a bus system containing multiple renewable energy sources, and traditional grid elements along different loads.

individual renewable source models are denoted in (24) and (25) where k and m represent the component ID. In the models ω and χ are input variables supported by the regression coefficients (a_k, b_k, c_m, d_m). Each wind turbine and PV module is modeled using a polynomial regression equation based on specific input parameters, such as wind speed ω for wind turbines and solar irradiance χ for PV modules. The total power output for a single MG P_{MG} is the sum of the power outputs from all wind turbines and PV modules within that microgrid. Extending this to multiple MGs, the overall total power output P_{total} is the sum of the power outputs from all wind turbines and PV modules across all microgrids, ensuring that each component is uniquely identified with an identical ID for easy access through the digital twin's cyber layer. This method is sustainable since it incorporates the computational costs of large networks as a predefined design consideration. Additionally, it models components based on their current lifecycle, ensuring relevance and applicability to current systems.

8. Conclusion

This article successfully tested the integration of a digital twin system in a microgrid operation. An islanded microgrid with DC and AC loads is employed in the experiment. Grid performance, uncertainty handling, and DT-controlled optimized operations are all tested, and the results are reported. As the experiment focuses on aspects such as operation and control, a modeling procedure for the final test cases is presented. Because the model is not universal, its execution in varied settings and with different components may necessitate a redesign for maximum accuracy.

This research demonstrates a technique for complicated system replication for optimal operation and control. Because the entire system is depicted in a single window, collaboration with digital twin technology improves system control and management. The most appealing aspect of this technology is that it is a responsive digital counterpart. As a result, it may be managed in real-time standard simulation-based features. The control system may vary depending on the scenario and the tolerances of various components. The future MG's operational needs, maintenance, data recording, and control are met by the digital twin models created, offering predictive performance data. This facilitates the optimization of generation, allowing for either maximizing output or dynamically adjusting generation components. Conducting additional tests and implementing them in larger systems could further enhance its reliability. Again, a legitimate concern is the declining efficiency of grid components after a certain lifecycle. To build an effective predictive model, it is essential to remodel or define a lifecycle metric for each component, encompassing both generation and control aspects. By doing so, the grid control can be optimized for long-term efficiency, ensuring that control algorithms maintain their reliability over time. Accordingly, our future focus will be on the impact of Decision-Time (DT)-based control on extensive generation and distribution networks to observe insights about the rapid transient state alteration of a DTEG with various load conditions and dynamic islanding of microgrids. Furthermore, exploring the impact of component lifecycles in the model is essential to ensure dynamic accuracy.

CRediT authorship contribution statement

Md. Mhamud Hussen Sifat: Writing – original draft, Visualization, Validation, Methodology, Formal analysis, Data curation, Conceptualization. **Safwat Mukarrama Choudhury:** Writing – original draft. **Sajal K. Das:** Validation, Supervision, Resources, Project administration. **Hemanshu Pota:** Writing – review & editing, Validation. **Fuwen Yang:** Writing – review & editing.

Declaration of competing interest

The authors declare that they have no known competing financial interests or personal relationships that could have appeared to influence the work reported in this paper.

Data availability

Data will be made available on request.

References

[1] Park H-A, Byeon G, Son W, Jo H-C, Kim J, Kim S. Digital twin for operation of microgrid: Optimal scheduling in virtual space of digital twin. Energies 2020;13(20):5504.

[2] Li Q, Cui Z, Cai Y, Su Y, Wang B. Renewable-based microgrids' energy management using smart deep learning techniques: Realistic digital twin case. Sol Energy 2023;250:128–38.

[3] Tenti P, Caldognetto T. On microgrid evolution to local area energy network (E-LAN). IEEE Trans Smart Grid 2017;10(2):1567–76.

[4] Ferahtia S, Houari A, Cioara T, Bouznit M, Rezk H, Djerioui A. Recent advances on energy management and control of direct current microgrid for smart cities and industry: A survey. Appl Energy 2024;368:123501.

[5] Vasilakis A, Zafeiratou I, Lagos DT, Hatziargyriou ND. The evolution of research in microgrids control. IEEE Open Access J Power Energy 2020;7:331–43.

[6] Venayagamoorthy GK, Sharma RK, Gautam PK, Ahmadi A. Dynamic energy management system for a smart microgrid. IEEE Trans Neural Netw Learn Syst 2016;27(8):1643–56.

[7] Harrold DJ, Cao J, Fan Z. Renewable energy integration and microgrid energy trading using multi-agent deep reinforcement learning. Appl Energy 2022;318:119151.

[8] Saeed MH, Fangzong W, Kalwar BA, Iqbal S. A review on microgrids' challenges & perspectives. IEEE Access 2021;9:166502–17.

[9] Faisal M, Hannan MA, Ker PJ, Hussain A, Mansor MB, Blaabjerg F. Review of energy storage system technologies in microgrid applications: Issues and challenges. IEEE Access 2018;6:35143–64.

[10] Marzal S, Salas R, González-Medina R, Garcerá G, Figueres E. Current challenges and future trends in the field of communication architectures for microgrids. Renew Sustain Energy Rev 2018;82:3610–22.

[11] Teimourzadeh S, Aminifar F, Davarpanah M. Microgrid dynamic security: Challenges, solutions and key considerations. Electr J 2017;30(4):43–51.

[12] Mirsaeidi S, Dong X, Shi S, Tzelepis D. Challenges, advances and future directions in protection of hybrid AC/DC microgrids. IET Renew Power Gener 2017;11(12):1495–502.

[13] Zhou M, Yan J, Feng D. Digital twin framework and its application to power grid online analysis. CSEE J Power Energy Syst 2019;5(3):391–8.

[14] Jiang Z, Lv H, Li Y, Guo Y. A novel application architecture of digital twin in smart grid. J Ambient Intell Humaniz Comput 2022;13(8):3819–35.

[15] Cheng T, Zhu X, Yang F, Wang W. Machine learning enabled learning based optimization algorithm in digital twin simulator for management of smart islanded solar-based microgrids. Sol Energy 2023;250:241–7.

[16] Tian H, Zhao H, Li H, Huang X, Qian X, Huang X. Digital twins of multiple energy networks based on real-time simulation using holomorphic embedding method, part II: Data-driven simulation. Int J Electr Power Energy Syst 2023;153:109325.

[17] Saad A, Faddel S, Youssef T, Mohammed OA. On the implementation of IoT-based digital twin for networked microgrids resiliency against cyber attacks. IEEE Trans Smart Grid 2020;11(6):5138–50.

[18] Fu Y, Huang Y, Hou F, Li K. A brief review of digital twin in electric power industry. In: 2022 IEEE 5th international electrical and energy conference. CIEEC, IEEE; 2022, p. 2314–8.

[19] Han J, Hong Q, Syed MH, Khan MAU, Yang G, Burt G, Booth C. Cloud-edge hosted digital twins for coordinated control of distributed energy resources. IEEE Trans Cloud Comput 2022.

[20] Danilczyk W, Sun Y, He H. ANGEL: An intelligent digital twin framework for microgrid security. In: 2019 North American power symposium. NAPS, IEEE; 2019, p. 1–6.

[21] Kim C, Dinh M-C, Sung H-J, Kim K-H, Choi J-H, Graber L, Yu I-K, Park M. Design, implementation, and evaluation of an output prediction model of the 10 MW floating offshore wind turbine for a digital twin. Energies 2022;15(17):6329.

[22] Tsado Y, Jogunola O, Olatunji FO, Adebisi B. A digital twin integrated cyber-physical systems for community energy trading. In: 2022 IEEE international conference on communications, control, and computing technologies for smart grids (smartGridComm). IEEE; 2022, p. 134–40.

[23] Darville J, Yavuz A, Runsewe T, Celik N. Effective sampling for drift mitigation in machine learning using scenario selection: A microgrid case study. Appl Energy 2023;341:121048.

[24] Cao W, Zhou L. Resilient microgrid modeling in digital twin considering demand response and landscape design of renewable energy. Sustain Energy Technol Assess 2024;64:103628.

[25] Pan M, Xing Q, Chai Z, Zhao H, Sun Q, Duan D. Real-time digital twin machine learning-based cost minimization model for renewable-based microgrids considering uncertainty. Sol Energy 2023;250:355–67.

[26] Natgunanathan I, Mak-Hau V, Rajasegarar S, Anwar A. Deakin microgrid digital twin and analysis of AI models for power generation prediction. Energy Convers Manage: X 2023;18:100370.

[27] Jiang H, Tjandra R, Soh CB, Cao S, Soh DCL, Tan KT, Tseng KJ, Krishnan SB. Digital twin of microgrid for predictive power control to buildings. Sustainability 2024;16(2):482.

[28] Padmawansa N, Gunawardane K, Madanian S, Than Oo AM. Battery energy storage capacity estimation for microgrids using digital twin concept. Energies 2023;16(12):4540.

[29] Meng F, Wang X. Digital twin for intelligent probabilistic short term load forecasting in solar based smart grids using shark algorithm. Sol Energy 2023;262:111870.

[30] You L, Zhu M. Digital twin simulation for deep learning framework for predicting solar energy market load in trade-by-trade data. Sol Energy 2023;250:388–97.

[31] Bian Y, Xie L, Ye J, Ma L, Cui C. Peer-to-peer energy sharing model considering multi-objective optimal allocation of shared energy storage in a multi-microgrid system. Energy 2024;288:129864.

[32] Shahzad S, Abbasi MA, Ali H, Iqbal M, Munir R, Kilic H. Possibilities, challenges, and future opportunities of microgrids: A review. Sustainability 2023;15(8):6366.

[33] Chakraborty S, Adhikari S. Machine learning based digital twin for dynamical systems with multiple time-scales. Comput Struct 2021;243:106410.

[34] Wang D, Fan R, Li Y, Sun Q. Digital twin based multi-objective energy management strategy for energy internet. Int J Electr Power Energy Syst 2023;154:109368.

[35] Sifat MMH, Choudhury SM, Das SK, Ahamed MH, Muyeen S, Hasan MM, Ali MF, Tasneem Z, Islam MM, Islam MR, et al. Towards electric digital twin grid: Technology and framework review. Energy AI 2023;11:100213.

[36] Bicocchi N, Fogli M, Giannelli C, Picone M, Virdis A. Requirements and design architecture for digital twin end-to-end trustworthiness. IEEE Internet Comput 2024.

[37] Bergs T, Gierlings S, Auerbach T, Klink A, Schraknepper D, Augspurger T. The concept of digital twin and digital shadow in manufacturing. Procedia CIRP 2021;101:81–4.

[38] Radanliev P, De Roure D, Nicolescu R, Huth M, Santos O. Digital twins: Artificial intelligence and the IoT cyber-physical systems in industry 4.0. Int J Intell Robot Appl 2022;6(1):171–85.

[39] Khan R, Tsiga N, Ghanem K. Building a digital twin for industrial internet of things with interoperability. In: 2022 moscow workshop on electronic and networking technologies. MWENT, IEEE; 2022, p. 1–5.

[40] Wen J, Gabrys B, Musial K. Towards digital twin-oriented complex networked systems: Introducing heterogeneous node features and interaction rules. PLoS One 2024;19(1):e0296426.

[41] Bariah L, Debbah M. The interplay of ai and digital twin: Bridging the gap between data-driven and model-driven approaches. IEEE Wirel Commun 2024.

[42] Lin J, Magnago F, Alemany JM. Optimization methods applied to power systems: current practices and challenges. Class Recent Aspects Power Syst Optim 2018;1–18.

[43] Arefifar SA, Alam MS, Hamadi A. A review on self-healing in modern power distribution systems. J Mod Power Syst Clean Energy 2023;11(6):1719–33.

[44] Rath S, Nguyen LD, Sahoo S, Popovski P. Self-healing secure blockchain framework in microgrids. IEEE Trans Smart Grid 2023;14(6):4729–40.

[45] baanders. Service limits - Azure Digital Twins — learn.microsoft.com. 2024, https://learn.microsoft.com/en-us/azure/digital-twins/reference-service-limits. [Accessed 18 July 2024].